International Journal of Technology 14(1) 206-218 (2023)
Received April 2021 / Revised May 2021 / Accepted July 2021

International Journal of Technology

http://ijtech.eng.ui.ac.id

Biodiesel Production from Free Fatty Acid using ZrO_2/Bagasse Fly Ash Catalyst

Fadilla Noor Rahma[1*], Arif Hidayat[1]

[1]*Chemical Engineering Department, Universitas Islam Indonesia, Jalan Kaliurang Km 14.5 Yogyakarta 55584, Indonesia*

Abstract. This study utilizes ZrO_2/Bagasse Fly Ash as a solid catalyst to convert Free Fatty Acid (FFA) from Palm Fatty Acid Distillate (PFAD) into biodiesel. The ZrO_2/Bagasse fly ash catalyst was characterized by several physicochemical techniques, i.e., N_2 adsorption-desorption, X-ray diffraction (XRD), and X-ray fluorescent (XRF). The catalyst was then applied for FFA esterification under different conditions. The highest FFA esterification conversion was 90.6%, which was reached at the optimal reaction condition as follows: methanol/PFAD mass ratio of 10:1; catalyst amount of 10 wt%; and reaction temperature of 60 ^oC. It was also found that the catalyst could be reused up to four times by an activation process. This study presented the Eley-Rideal kinetic model to describe the reaction mechanism. The model demonstrated an excellent fit to the experimental result with an R^2 value of 0.99, showing that Eley-Rideal is a valid model to describe the reaction and that the surface reaction step acts as the rate-determining step. Additionally, the reaction kinetics and adsorption equilibrium parameters were determined using non-linear regression. The correlation between the parameters with temperature was evaluated using Arrhenius and van't Hoff equations.

Keywords: Bagasse fly ash; Biodiesel; Catalyst; Esterification; Free fatty acid

1. Introduction

In recent years, the research for renewable alternative sources of energy has been strongly supported to minimize reliance on fossil fuels and address environmental issues (Susanto *et al.,* 2020, Sudibandriyo and Putri, 2020). Biodiesel has been gaining more attention due to several advantages, such as its biodegradability, non-toxicity, and ability to be applied as a petroleum diesel replacement with no required engine modification. Moreover, biodiesel is environmentally friendly because it has the potential to significantly reduce global warming and could be obtained from renewable resources (Abdullah *et al.,* 2017). The majority of feedstocks utilized in the production of biodiesel are derived from either plant oils or animal fats.

Biodiesel is chemically known as fatty acid mono-alkyl esters (FAME). It is generally synthesized by transesterification of the triglycerides or esterification of free fatty acids commonly discovered in renewable resources. Two types of conventional catalysts applied in biodiesel synthesis include homogeneous acid catalysts and homogeneous alkaline catalysts (Saksono *et al.,* 2019). However, homogeneous catalysts have several

*Corresponding author's email: fadilla.noor@uii.ac.id, Tel.: +62-274-895287
doi: 10.14716/ijtech.v14i1.4873

disadvantages due to their highly toxic, corrosive, and flammable nature. In addition, they also require advanced separation for product recovery, incurring additional operational costs, a large volume of wastewater, and serious environmental problems (Bhatia *et al.,* 2021).

Studies on heterogeneous catalysts are gaining more interest due to their advantages over homogeneous catalysts. Heterogeneous catalysts offer operational benefits due to their non-corrosive nature. Additionally, the use of heterogeneous catalysts also eliminates the necessity for advanced product separation and enables catalyst reuse. Consequently, the associated costs, energy consumption, and quantity of wastewater produced can be drastically reduced. Many researchers have investigated solid catalysts for esterification reactions to biodiesel production. However, the main limitation of chemical-based heterogeneous catalysts lies in their low stability and high production costs (Bhatia *et al.,* 2021).

To overcome these problems, recent studies have been focusing on low-cost biomass-based heterogeneous catalysts as an alternative for biodiesel production. This type of catalyst can be easily produced from renewable biomass resources, eliminating the costly preparation steps required for chemical-based catalysts. Biomass-based catalysts have also demonstrated high efficiency, catalytic activity, and stability (Bhatia *et al.,* 2021). In addition, this type of catalyst is environmentally friendly since it can be derived from renewable and abundantly available biomass sources, ensuring its supply sustainability. Numerous studies have reported the utilization of various biomass materials as solid catalysts for biodiesel production, such as animal bones and shells (Verziu *et al.,* 2011), biomass ashes (Chouhan and Sarma, 2013), activated carbon-supported catalysts (Lee *et al.,* 2014), biomass residues (Fu *et al.,* 2013), and biochar (Kastner *et al.,* 2012).

Bagasse fly ash (BFA) is an agricultural waste produced when sugarcane bagasse is burned following the sugar extraction process in sugar and ethanol plants. It is a potential source of catalyst support due to its high content of natural silica (Falk *et al.,* 2019). A BFA catalyst is suitable for the esterification process of feedstocks having high FFA content (Mukti, Sutrisno, and Hidayat, 2018). Since BFA is produced in abundant amounts, its utilization as a catalyst for biodiesel production would help reduce the environmental pollution and disposal problem (Mutalib *et al.,* 2020). The biodiesel production process will benefit economically from the simple preparation of BFA catalyst as well as the low material and production costs.

The performance of the BFA catalyst can be improved by impregnation using ZnO_2, which has the advantage of chemical, thermal, and mechanical stability, as well as unique acidic properties. It has been asserted that zirconia-impregnated catalysts are material of interest due to their amphoteric nature, which allows them to perform as either an acid or a base catalyst. Furthermore, the acidity of Zirconia can be enhanced by modification using acid promoters such as sulfuric acid (Saravanan *et al.,* 2016), ammonium sulfate (Rattanaphra *et al.,* 2012), and chlorosulfonic acid (Zhang *et al.,* 2014). The use of ZnO_2 is regarded as one of the most superior heterogeneous acid catalysts among other options, such as titanium oxide, tin oxide, and sulfonated carbon catalysts (Ma'rifah *et al.,* 2019).

Currently, more attention has been given to the economic feasibility of biodiesel production. Other than the catalyst, another major cost contributing to the overall biodiesel production is the raw material cost (Jamil *et al.,* 2018). To obtain a more attractive biodiesel sales price, the use of low-cost material should be encouraged over the use of refined vegetable oils. Recently, the usage of second-generation biodiesel, including used cooking oil, non-edible oils, and animal fats is increasingly favored because they do not compete with food and energy resources. The utilization of low-cost non-edible oils also significantly

reduces production costs, thus improving the economic feasibility of biodiesel production (Pant *et al.,* 2019).

Palm Fatty Acid Distillate (PFAD), with 98% content of free fatty acid (FFA) (Ibrahim *et al.,* 2020), is a prospective feedstock for biodiesel production. PFAD is mostly obtained as the refinery by-product of crude palm oil (CPO). Commonly, 32.5 kgs of PFAD is generated for each tonne of processed CPO (3.25 wt.% of CPO) (Kapor *et al.,* 2017). In 2019, CPO output reached 47,180,000 tons, which resulted in approximately 1,533,350 tons of PFAD. These estimates are projected to rise by 5–7% annually through 2030 (Badan Pusat Statistik, 2020). In Indonesia, the price of PFAD is one-fourth that of palm oil, making it an attractive option for reducing the cost of biodiesel production. Without proper disposal, the increasing use of PFAD as animal feed could cause environmental hazards.

In this study, the FFA content in PFAD was esterified over Zirconia metal loaded on sugarcane bagasse fly ash (BFA) as a solid acid catalyst. The catalyst characteristics analysis was performed using Nitrogen adsorption-desorption, X-Ray Diffraction (XRD), and X-Ray Fluorescent (XRF). The catalyst performance was observed by varying the reaction temperatures, methanol to PFAD molar ratios, and catalyst loading. In addition, the reusability and reaction kinetics of the catalyst were investigated.

2. Methods

2.1. Materials

Palm Fatty Acid Distillate (PFAD) was obtained from a palm oil refinery in East Kalimantan Province, Indonesia. Bagasse fly ash (BFA) was obtained from PT Madu Baru, Bantul regency, D.I. Yogyakarta Province. Zirconyl chloride octahydrate ($ZrOCl_2.8H_2O$, Aldrich, 99%), was used as the source of the metals. Methanol (Merck & Co) was purchased from a local supplier in Yogyakarta Province.

2.2. Catalyst Synthesis

Prior to use, the BFA was cleaned using distilled water to remove impurities, and then the sample was dried at 110 ^oC overnight. The dried BFA was sieved to obtain particles sized less than 1 μm. The catalyst synthesis was conducted in the following steps: (i) Firstly, the BFA was dissolved in 0.5 N sulfuric acid solution to reduce the internal pore impurities; (ii) The activated BFA was then washed with distilled water up to the point when the wash water was free from sulfate ions and the pH of the water was neutral; (iii) The activated BFA was prepared using incipient wetness impregnation with Zirconium(IV) oxychloride octahydrate ($ZrOCl_4.8H_2O$), which was dissolved into 100 mL of distilled water, then added with the activated BFA; (iv) Afterward, the mixture was stirred in a three-neck flat bottom flask put on a hot plate magnetic stirrer equipped with a reflux condenser. This was completed vigorously at the reflux temperature overnight; (v) Following the impregnation, the catalyst was separated by filtration; (vi) Finally, the catalyst was calcined in a muffle furnace at 110 ^oC for 4 hours. The catalyst characteristics were analyzed by utilizing Nitrogen adsorption-desorption, X-Ray Diffraction (XRD), and X-ray fluorescent (XRF).

2.3. The Catalyst Performances

The esterification reaction was conducted by mixing the PFAD, methanol, and ZrO_2/bagasse fly ash catalyst in a batch reactor equipped with a temperature indicator, condenser, and hot plate magnetic stirrer. After the reaction, the catalyst was filtered out of the product mixture. Decantation was then conducted to separate the alcohol phase (excess methanol and water) from the organic phase (methyl esters). The remaining methanol in the methyl ester phase was evaporated in the oven for 4 h. The effect of temperature (30;

40; 50; and 60 °C), catalyst amount (1; 2.5; 5; and 10 wt.% of PFAD), and methanol/PFAD mole ratio (4/1; 6/1; 8/1; 10/1) were investigated.

The FFA conversion was determined using Equation (1), where $FFA_{initial}$ represents the FFA value of the feedstock and $FFA_{product}$ denotes the FFA value of the organic phase.

$$\text{FFA conversion (\%)} = \frac{FFA_{initial} - FFA_{product}}{FFA_{initial}} \quad (1)$$

2.4. Catalyst Reusability

The used catalysts were filtered out of the product mixture and collected. Methanol was used to wash the catalyst and remove the remaining residues of oil. This was followed by washing with hexane to remove both polar and non-polar components. Lastly, the used catalyst was oven-dried at the temperature of 100 °C for 12 h, before being reused in the subsequent round of reaction.

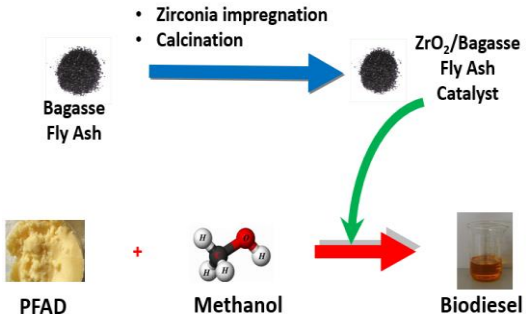

Figure 1 Research Method

2.5. Kinetic Modelling and Parameter Evaluation

The esterification of PFAD and methanol to form biodiesel is represented by Equation (2), where F, M, E, and W describe FFA, methanol, FAME, and water, respectively.

$$RCOOH + CH_3OH \leftrightarrow RCOOCH_3 + H_2O \quad (2)$$

$$(F) + (M) \leftrightarrow (E) + (W)$$

This study proposes the Eley-Rideal kinetic model to describe the reaction mechanism of FFA and methanol esterification using ZrO_2/BFA as a solid catalyst. The model assumes that only one of the reactants is adsorbed on the catalyst active site, whereas the other reactant interacts with the adsorbed species directly from the bulk liquid phase. In this particular case, methanol is considered the adsorbed species (Ilgen, 2014). The mechanism involves the following steps, with S denoting the catalyst's vacant active site:

$$M + S \underset{k_{-A}}{\overset{k_A}{\leftrightarrow}} M \cdot S \quad (3)$$

$$F + M \cdot S \underset{k_{-S}}{\overset{k_S}{\leftrightarrow}} E + W \cdot S \quad (4)$$

$$W \cdot S \underset{k_{-D}}{\overset{k_D}{\leftrightarrow}} W + S \quad (5)$$

The methanol adsorption, the surface reaction, and the water desorption are described by equations (3) through (5), respectively. The slow surface reaction between the adsorbed methanol and FFA in the liquid phase is considered to be the rate-determining step (RDS) (Pino *et al.,* 2018). The Eley-Rideal model considered the following assumptions: (a) the

mass transfer limitation is negligible due to the high agitation which ensures the homogeneity of the reactant mixture; (b) the catalytic activity on the entire catalyst surface is equal; (c) the adsorption and desorption steps of both reactant and product are at equilibrium; (d) the diffusion process of both reactant and product can be neglected. Based on these assumptions, the rate of FFA and methanol esterification on the solid catalyst can be calculated as follows:

$$-r_S = \frac{K_1\left(K_A C_M C_F - \frac{K_D}{K_S} C_W C_E\right)}{1 + K_A C_M + K_D C_W} \quad (6)$$

In Equation (6), K_A, K_S, and K_D respectively represent the equilibrium constants of the methanol adsorption, surface reaction, and water adsorption steps ($K_A = k_A/k_{-A}$; $K_S = k_S/k_{-S}$; and $K_D = k_{-D}/k_D$). In the kinetic constant ($K_1 = C_T.k_S$), C_T denotes the total concentration of the catalyst's active sites and k_S is the surface reaction rate constant. By minimizing the Sum of Squares Error (SSE) between the experimental data and the proposed model, the kinetics and equilibrium constants in equation (6) can be evaluated. Equation (7) is utilized, where $X_{F\,Exp}$ denotes the FFA conversion obtained from the experiment and $X_{F\,Calc}$ represents the FFA conversion calculated using the proposed model.

$$SSE = \sum \left(X_{F\,Exp} - X_{F\,Calc}\right)^2 \quad (7)$$

The temperature dependence of the kinetic constants K_1 can be described using the Arrhenius equation (8). Meanwhile, the temperature correlation with surface reaction equilibrium constant (K_S) and adsorption equilibrium constants (K_A and K_D) are described using the van't Hoff equation, presented in Equations (9) and (10), respectively (Zavrazhnov *et al.,* 2019).

$$K_1 = A \exp\left(\frac{-E_a}{RT}\right) \quad (8)$$

$$K_S = K_{S0} \exp\left(\frac{-\Delta H_R^\circ}{RT}\right) \quad (9)$$

$$K_i = K_{i0} \exp\left(\frac{-\Delta H_i^\circ}{RT}\right) \quad (10)$$

In Equation (8), A is the preexponential factor, L/(g_{cat} s); E_a is the activation energy, J/mol; R is the universal gas constant; and T is the temperature, K. In Equation (9), K_{S0} is the integration constant; $-\Delta H_R^\circ$ is the reaction enthalpy, J/mol; R is the universal gas constant; and T is the temperature, K. Whereas for Equation (10), K_i is the adsorption equilibrium constant of component i, L/mol; K_{i0} is the integration constant, L/mol; $-\Delta H_i^\circ$ is the adsorption enthalpy, J/mol; R is the universal gas constant; and T is the temperature, K.

3. Results and Discussion

3.1. Catalyst Characteristics

Table 1 depicts the results of the characterization of catalysts. The average pore size diameter and BET surface area of the activated BFA are 2.29 nm and 55.74 m^2/g, respectively; while those of the ZrO_2/BFA catalyst are 3.17 nm and 31.51 m^2/g, respectively. According to the BET analysis, the pore size diameter of the synthesized catalyst falls in the mesoporous range, which is in the range of 2.0-50 nm. This mesoporous structure can decrease the intraparticle diffusional limitations which are related to the molecular sieve-based acid catalysts.

During the Zirconia impregnation on the activated BFA, Zirconia is anchored to the internal surface of the catalyst pore by incipient wetness impregnation method followed by calcination to form metal oxides. The latter process can block access to the internal pores, causing smaller pores to be inaccessible, which results in a decreasing specific surface area. In addition, there was an increase in the pore volume and size of the ZrO_2/BFA catalyst, leading to a lower catalyst surface area.

Table 1 Characteristics of activated BFA and ZrO_2/BFA catalysts

Characteristics	Activated BFA	ZrO_2/BFA catalyst
BET surface area ($m^2\ g^{-1}$)	55.74	31.51
Average pore size diameter (nm)	2.29	3.17
total pore volume ($cm^3\ g^{-1}$)	0.05413	0.1055

Figure 2 demonstrates the XRD results in the activated BFA and ZrO_2/BFA catalyst. The XRD pattern of pure ZrO_2 displays typical diffraction peaks at 2θ = 27.78°, 31.2°, and 49.54° which is a monoclinic crystal system. Meanwhile, BFA comprises tridymite and α-cristobalite crystalline structure at 2θ values of 21.8°, 28.4°, 31.3°, and 36.0°. For the ZrO_2/BFA catalyst, the value of 2θ in the range of 20-40° indicates the high amorphous content of the catalyst. Based on the XRD pattern, the peak characteristics of the Zirconia phase are not exhibited in the analysis results. The calcination process increased the interaction between BFA and zirconia metal, as demonstrated by the appearance of several new peaks in the XRD pattern of the catalyst. Nonetheless, the specific crystal structure of ZnO_2 has not yet been determined.

The analysis using XRF (X-Ray Fluorescence) was applied to analyze the formula of the solid catalyst. EDX spectrometry was applied to determine the Zirconia content in ZrO_2/BFA catalyst and activated BFA catalyst. The results of the EDX analysis showed that the ZrO_2/BFA catalyst contained 3.82 wt% Zirconia. Meanwhile, the presence of Zirconia metal was not detected in the bagasse fly ash. It can be concluded that the impregnation process successfully attached Zirconia molecules to the BFA catalyst.

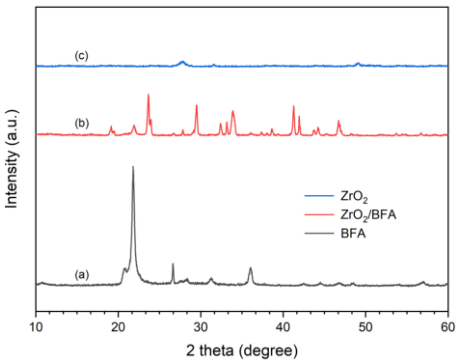

Figure 2 XRD pattern of: (a) BFA, (b) ZrO_2/BFA catalyst, and (c) pure ZrO_2

3.2. Effect of Molar Ratio

The molar ratio represents the comparison between the total moles of methanol and FFA in the PFAD, which is an essential aspect of biodiesel production. In this study, the effect of the methanol/PFAD molar ratio on the FFA conversion was investigated by varying the ratio from 4/1 to 10/1. The experiment was performed at the reaction temperature of 60 ^oC, catalyst loading of 10 wt.% of PFAD, and reaction time of 2 hours. As shown in Figure 3 (a), the FFA conversion consistently increased as the methanol/PFAD molar ratio was added. Theoretically, the stoichiometric methanol/PFAD molar ratio is 1:1. The addition of excess methanol shifts the reaction equilibrium towards the formation of FAME, thus

increasing the FFA conversion (Song *et al.,* 2010). In addition, a higher methanol amount also causes higher collision among the reactants, enhancing the rate of product formation (Augustia *et al.,* 2018). The most remarkable change is observed in the ratio increase from 4/1 to 6/1, which improved the FFA conversion from 51.1% to 77.3%, whereas higher methanol/PFAD ratio leads to less significant increase of the FFA conversion. This is partly attributed to the limited amount of active catalytic surface, which reaches a higher degree of saturation with more addition of methanol. Another contributing factor is the accumulation of the adsorbed alcohol on the catalyst surface, which counterbalances the effect of the shifted reaction equilibrium (Jiang *et al.,* 2013). The highest FFA conversion of 90.6% was obtained at the methanol/PFAD ratio of 10/1.

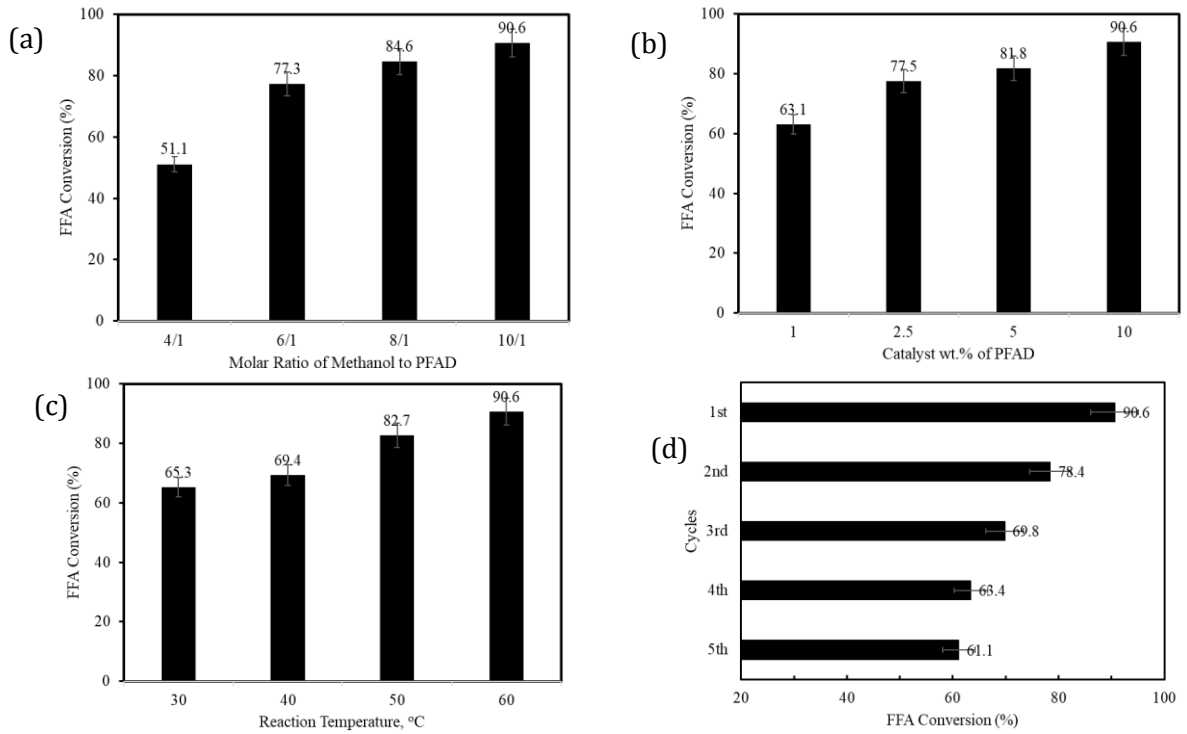

Figure 3 Effect of (a) molar ratio of methanol to PFAD; (b) catalyst wt.% of PFAD; (c) reaction temperature; and (d) catalyst reuse on FFA conversion

3.3. Effect of Catalyst Loading

Figure 3 (b) depicts the results of the ZrO_2/BFA catalyst performance test for the FFA esterification reaction with varying amounts of PFAD catalyst, ranging from 1 to 10 wt.% of PFAD. The observation was performed at the constant temperature of 60 °C, methanol to PFAD molar ratio of 10/1, and reaction time of 2 h. Following the addition of the catalyst amount, the resulting figure demonstrates a rising trend in FFA conversion. As the catalyst loading varied from 1 to 2.5; 5; and 10 wt.% of PFAD, the FFA conversion increased from 63.1% to 77.5%, 81.8%, and 90.6% respectively. The addition of catalyst increases the number of available active catalyst sites, resulting in a faster reaction rate and a higher FFA conversion (Ilgen, 2014). A similar effect is documented in the previous studies in the esterification of FFA using different types of catalysts (Gan *et al.,* 2012).

3.4. Effect of Reaction Temperature

Four different reaction temperatures (30, 40, 50, and 60 °C) were selected to investigate the impact of reaction temperature on the esterification of PFAD with methanol. The other operating parameters were maintained constant at the methanol/PFAD molar ratio of 10/1; catalyst loading of 10 wt.% of PFAD; and reaction time of 2 h. Figure 3 (c)

shows that the FFA conversion demonstrated a significant dependence on the reaction temperature. The figure indicates that FFA conversion increased from 65.3% to 90.6% as the reaction temperature was raised from 30 to 60 °C. This trend is attributed to several contributing factors, including the endothermic nature of the reaction. From the thermodynamic point of view, an endothermic reaction is favored by the higher temperature, which will push the reaction towards the formation of the product (Ilgen, 2014). It should also be noted that the immiscible nature of PFAD and methanol produced a three-phase liquid-liquid-solid system consisting of PFAD-methanol-catalyst. In this type of system, the reaction rate would be substantially limited to the mass transfer rate of reactant molecules among the three phases. The increase in temperature affects the kinetics of the reaction by providing more kinetic energy to the reactant molecules, accelerating the mass transfer rate among the three phases, and enhancing the rate of reaction (Liu *et al.,* 2014). Furthermore, a higher temperature reduces the number of water molecules on the catalytic surface and prevents them from bonding strongly to the active catalytic sites (Zhang *et al.,* 2014; Jiang *et al.,* 2013). As previously discovered by other researchers, these variables result in an increasing trend of FFA conversion as temperature increases (Augustia *et al.,* 2018; Liu *et al.,* 2014).

3.5. Catalyst Reusability

The reusability of the catalyst is an essential factor since it directly influences the economics of the process (Ilgen, 2014). In this study, the catalyst was reapplied several times for the PFAD and methanol esterification to examine the catalyst reusability. The catalyst was filtered and treated (including drying and washing) before being utilized in the subsequent reaction cycle. In repeated cycles of esterification, the optimum condition is a reaction temperature of 60 °C, a molar ratio of 10/1 between methanol and PFAD, a catalyst loading of 10 wt% of PFAD, and a reaction time of 2 h. Figure 3 (d) shows the result of applying the catalyst for four cycles. The figure shows a notable decrease in the catalytic activity as the catalyst was reused in each cycle. This indicates the leaching of catalyst active sites, signifying that fresh catalysts should be added to the mixture to maintain the reaction performance.

3.6. Kinetic Modelling and Parameter Evaluation

In this study, the Eley-Rideal kinetic model was proposed to describe the reaction mechanism of PFAD and methanol esterification over the ZrO_2/BFA solid catalyst. The Eley-Rideal describes a catalytic reaction mechanism in which one of the reactants is chemisorbed and the other one is not (Prins, 2018). This model has been previously proposed to describe FFA esterification to biodiesel in previous studies (Augustia *et al.,* 2018; Ilgen, 2014; Tesser *et al.,* 2010; Tesser *et al.,* 2009). In this paper, the Eley-Rideal model considers the adsorption and desorption of one of the reactants (methanol) and one of the products (water), while neglecting the intraparticle diffusional limitation. The surface reaction of the adsorbed methanol with FFA in the bulk liquid phase is regarded as the rate-determining step. The value of the parameters in Equation (5) was determined by minimizing the SSE between the experimental data of FFA conversion and the modeling result. To examine this, the reaction was performed under the optimal conditions: a methanol/PFAD molar ratio of 10/1; catalyst loading of 10 wt.% of PFAD; and a reaction time of 2 h. The temperatures of 30, 40, 50, and 60 °C were selected to observe the correlation between kinetic parameters and reaction temperature.

Figure 4 demonstrates an excellent correlation between the experimental data and the Eley-Rideal model (R^2 = 0.99) as indicated by the result. This demonstrates the validity of the Eley-Rideal mechanism with surface reaction as the rate-determining step, signifying

that the model is accurate for describing PFAD and methanol esterification over ZrO_2/BFA catalyst. The calculated parameters are summarized in Table 2.

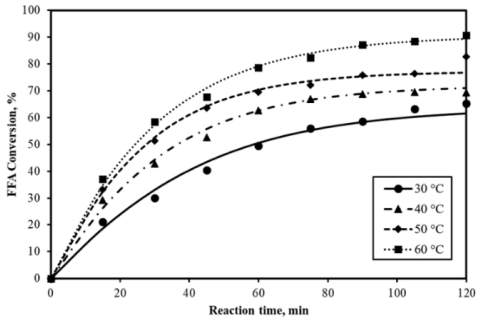

Figure 4 FFA conversion at different temperatures: Eley-Rideal fitting to experimental data

Table 2 Kinetic parameters of PFAD and methanol esterification on ZrO_2/BFA catalyst

Temperature °C	K_1 L/(g_{cat} min)	K_S	K_A L/mol	K_D L/mol
30	0.7607	0.2522	1.5017	3.0164
40	0.8174	0.2846	2.0723	2.8713
50	0.9783	0.3586	2.2296	2.7274
60	1.0643	0.6772	2.2077	1.5712

The parametric evaluation results in Table 2 suggest a correlation between the obtained parameters with the reaction temperature. The reaction kinetic constant K_1 was found to be positively correlated with temperature, due to the endothermic nature of the esterification reaction. As discussed in the previous section, temperature increase accelerates the rate of endothermic processes (Ilgen, 2014), which is mathematically represented by the increase in kinetic constant value. The same trend is observed for the equilibrium constant of the surface reaction, which is denoted by K_S. The value of K_S increases as the temperature rises, indicating that a higher temperature drives the surface reaction toward the formation of the products. Similarly, the methanol equilibrium adsorption constant K_A also increases as the temperature gets higher, implying that methanol adsorption onto the ZrO_2/BFA catalytic surface is also an endothermic process. The energy required to overcome the reaction's endothermic nature was provided by heating during the reaction. In contrast, the water adsorption equilibrium constant K_D is negatively affected by the temperature, indicating that water is adsorbed exothermically on the catalyst surface.

Figures 5 (a), (b), (c), and (d) displayed the plots for K_1, K_S, K_A, and K_D, respectively. The values of A, K_{S0}, and K_{i0} were obtained from the intercept of the straight line, whereas the values of E_a, $\Delta H_S°$, and $\Delta H_i°$ were calculated from the line slope. Table 3 presents a summary of the results.

Table 3 Parametric evaluation results from Arrhenius and Van't Hoff equations

Evaluated Constants	Calculated Parameters	Value
K_1	Preexponential factor	A = 38.7798 L/(g_{cat} s)
	Activation energy	E_a = 9.9389 kJ/mol
K_S	Integration constant	K_{S0} = 8319.0222
	Enthalpy of reaction	$\Delta H_S°$ = 26.4884 kJ/mol
K_A	Integration constant	K_{A0} = 104.7315 L/mol
	Enthalpy of adsorption (methanol)	$\Delta H_A°$ = 10.4731 kJ/mol
K_D	Integration constant	K_{D0} = 0.0046 L/mol
	Enthalpy of adsorption (water)	$\Delta H_D°$ = -16.5603 kJ/mol

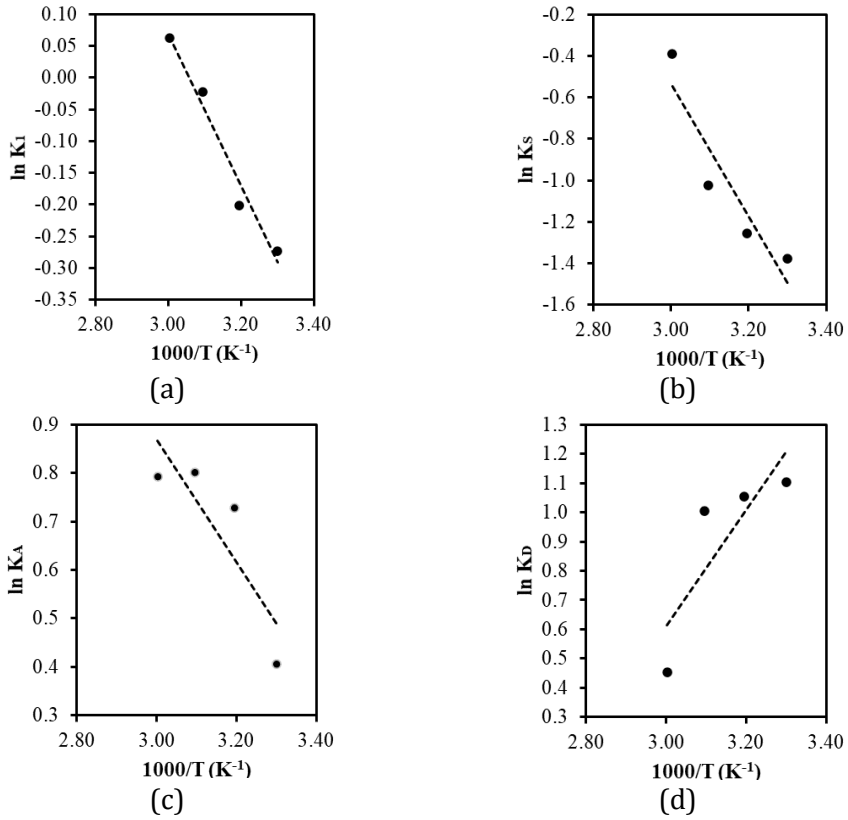

Figure 5 The correlation of temperature with (a) K_1; (b) K_S; (c) K_A; and (d) K_D: Fitting to Arrhenius and Van't Hoff equations parameters

The relationship between the obtained kinetic and equilibrium parameters with the temperature was assumed to follow Arrhenius and van't Hoff correlations (Ketzer and de Castilhos, 2021). Therefore, they can be evaluated by plotting (ln K) against (1/T), based on the linearized Arrhenius and van't Hoff equations (Equations 8 to 10).

4. Conclusions

Bagasse fly ash (BFA) was used as catalyst support for biodiesel production from Palm Fatty Acid Distillate. The catalyst was prepared by activation of the BFA followed by impregnation of Zirconia metals using Zirconium(IV) oxychloride octahydrate salt solution. The catalyst was characterized using N_2 adsorption-desorption, X-ray diffraction (XRD), and X-ray fluorescent (XRF). A maximum FFA conversion of 90.6% was obtained at the following operation conditions: Reaction temperature of 60 ^{o}C; methanol to PFAD ratio of 10/1; catalyst loading of 10 wt.% of PFAD; and reaction temperature of 2 h. During four cycles of esterification reaction, a 14-37% decrease in FFA conversion was observed. The reaction kinetic follows the Eley-Rideal kinetic mechanism. The kinetic and adsorption equilibrium parameters were evaluated and their correlation with temperature was described using Arrhenius and van't Hoff equations. Future research should investigate the utilization of BFA as a solid catalyst in the esterification of FFA from PFAD using a continuous process, which will be a significant step towards a more sustainable, low-cost, and environmentally friendly biodiesel production process.

References

Abdullah, S.H.Y.S., Hanapi, N.H.M., Azid, A., Umar, R., Juahir, H., Khatoon, H., Endut, A., 2017. A review of biomass-derived heterogeneous catalyst for - sustainable biodiesel production. *Renewable and Sustainable Energy Reviews,* Volume 70**,** pp. 1040–1051

Augustia, V., Djalal, R., Sutrisno, B., Hidayat, A., 2018. Published. Kinetic study of free fatty acid in Palm Fatty Acid Distillate (PFAD) over sugarcane bagasse catalyst. *In:* IOP Conference Series: Earth and Environmental Science, IOP Publishing, p. 012065

Badan Pusat Statistik. 2020. Statistik Kelapa Sawit Indonesia 2019 *(Indonesian Palm Oil Statistics 2019)*. Available online at: https://www.bps.go.id/publication/2020/11/30/36cba77a73179202def4ba14/statistik-kelapa-sawit-indonesia-2019.html, Accessed on October 2021

Bhatia, S.K., Bhatia, R.K., Jeon, J.-M., Pugazhendhi, A., Awasthi, M.K., Kumar, D., Kumar, G., Yoon, J.-J., Yang, Y.-H., 2021. An overview of advancements in biobased transesterification methods for biodiesel production: Oil resources, extraction, biocatalysts, and process intensification technologies. *Fuel,* Volume 285**,** p. 119117

Chouhan, A.P.S., Sarma, A.K., 2013. Biodiesel production from Jatropha curcas L. oil using Lemna perpusilla Torrey ash as heterogeneous catalyst. *Biomass and Bioenergy,* Volume 55**,** pp. 386–389

Falk, G., Shinhe, G., Teixeira, L., Moraes, E. De Oliveira, A.N., 2019. Synthesis of silica nanoparticles from sugarcane bagasse ash and nano-silicon via magnesiothermic reactions. *Ceramics International,* Volume 45(17)**,** pp. 21618–21624

Fu, X., Li, D., Chen, J., Zhang, Y., Huang, W., Zhu, Y., Yang, J., Zhang, C., 2013. A microalgae residue based carbon solid acid catalyst for biodiesel production. *Bioresource Technology,* Volume 146**,** pp. 767–770

Gan, S., Ng, H. K., Chan, P. H., Leong, F. L., 2012. Heterogeneous free fatty acids esterification in waste cooking oil using ion-exchange resins. *Fuel Processing Technology,* Volume 102**,** pp. 67–72

Ibrahim, S.F., Asikin-Mijan, N., Ibrahim, M.L., Abdulkareem-Alsultan, G., Izham, S.M., Taufiq-Yap, Y., 2020. Sulfonated functionalization of carbon derived corncob residue via hydrothermal synthesis route for esterification of palm fatty acid distillate. *Energy Conversion and Management,* Volume 210**,** p. 112698

Ilgen, O., 2014. Investigation of reaction parameters, kinetics and mechanism of oleic acid esterification with methanol by using Amberlyst 46 as a catalyst. *Fuel Processing Technology,* Volume 124**,** pp. 134–139

Jamil, F., Myint, M.T.Z., Al-Hinai, M., Al-Haj, L., Baawain, M., Al-Abri, M., Kumar, G., Atabani, A., 2018. Biodiesel production by valorizing waste Phoenix dactylifera L. Kernel oil in the presence of synthesized heterogeneous metallic oxide catalyst (Mn@ MgO-ZrO2). *Energy Conversion and Management,* Volume 155**,** pp. 128–137

Jiang, Y., Lu, J., Sun, K., Ma, L., Ding, J., 2013. Esterification of oleic acid with ethanol catalyzed by sulfonated cation exchange resin: Experimental and kinetic studies. *Energy Conversion and Management,* Volume 76**,** pp. 980–985

Kapor, N.Z.A., Maniam, G.P., Rahim, M.H.A., Yusoff, M.M., 2017. Palm fatty acid distillate as a potential source for biodiesel production-a review. *Journal of Cleaner Production,* Volume 143**,** pp. 1–9

Kastner, J.R., Miller, J., Geller, D.P., Locklin, J., Keith, L.H., Johnson, T., 2012. Catalytic esterification of fatty acids using solid acid catalysts generated from biochar and activated carbon. *Catalysis Today,* Volume 190**,** pp. 122–132

Ketzer, F., De Castilhos, F., 2021. An assessment on kinetic modeling of esterification reaction from oleic acid and methyl acetate over USY zeolite. *Microporous and Mesoporous Materials,* Volume 314**,** p. 110890

Lee, A.F., Bennett, J.A., Manayil, J.C., Wilson, K., 2014. Heterogeneous catalysis for sustainable biodiesel production via esterification and transesterification. *Chemical Society Reviews,* Volume 43**,** pp. 7887–7916

Liu, W., Yin, P., Zhang, J., Tang, Q., Qu, R., 2014. Biodiesel production from esterification of free fatty acid over PA/NaY solid catalyst. *Energy conversion and management,* Volume 82**,** 83–91

Ma'rifah, Y.N., Nata, I.F., Wijayanti, H., Mirwan, A., Irawan, C., Putra, M.D. Kawakita, H., 2019. One-step Synthesis to enchance the acidity of a biocarbon-based sulfonated solid acid catalyst. *International Journal of Technology*, Volume 10(3), pp. 512-520

Mukti, N., Sutrisno, B., Hidayat, A., 2018. Published. Production of Biodiesel by Esterification of Free Fatty Acid over Solid Catalyst from Biomass Waste. *In:* IOP Conference Series: Materials Science and Engineering, IOP Publishing, p. 012005

Mutalib, A.a.A., Ibrahim, M.L., Matmin, J., Kassim, MF., Mastuli, M.S., Taufiq-Yap, Y.H., Shohaimi, N.a.M., Islam, A., Tan, Y.H., Kaus, N.H.M., 2020. SiO_2-Rich sugar cane bagasse ash catalyst for transesterification of palm oil. *BioEnergy Research,* Volume 13**,** pp. 986–997

Pant, D., Misra, S., Nizami, A.-S., Rehan, M., Van Leeuwen, R., Tabacchioni, S., Goel, R., Sarma, P., Bakker, R., Sharma, N., 2019. Towards the development of a biobased economy in Europe and India. *Critical reviews in biotechnology,* Volume 39**,** pp. 779–799

Pino, L., Recupero, V., Hernández, A., 2018. A useful excel-based program for kinetic model discrimination. *ChemEngineering,* Volume 2(4)**,** p. 57

Prins, R., 2018. Eley–Rideal, the other mechanism. *Topics in Catalysis*, Volume 61(9), p. 714-721

Rattanaphra, D., Harvey, A.P., Thanapimmetha, A., Srinophakun, P., 2012. Simultaneous transesterification and esterification for biodiesel production with and without a sulphated zirconia catalyst. *Fuel,* Volume 97**,** pp. 467–475

Saksono, N., Junior, A. B., Anditashafardiani, R., Muharam, Y., 2019. Effect of anode depth in synthesis of biodiesel using the anodic plasma electrolysis method. *International Journal of Technology,* Volume 10(3*),* pp. 491-501

Saravanan, K., Tyagi, B., Shukla, R.S., Bajaj, H. C., 2016. Solvent free synthesis of methyl palmitate over sulfated zirconia solid acid catalyst. *Fuel,* Volume 165**,** 298–305

Song, C., Qi, Y., Deng, T., Hou, X., Qin, Z., 2010. Kinetic model for the esterification of oleic acid catalyzed by zinc acetate in subcritical methanol. *Renewable energy,* Volume 35(3)**,** 625–628

Sudibandriyo, M., Putri, F.A., 2020. The effect of various zeolites as an adsorbent for bioethanol purification using a fixed bed adsorption column. *International Journal of Technology,* (11)**,** 1300–1308

Susanto, H., Fahmi, Y., Hutami, A.T., Hadi, Y.T., 2020. Effects of fly ash loading on the characteristics of PVC-based cation exchange membranes for reverse electrodialysis. *International Journal of Technology,* Volume 11(3)**,** pp. 544–553

Tesser, R., Casale, L., Verde, D., Di Serio, M., Santacesaria, E., 2009. Kinetics of free fatty acids esterification: Batch and loop reactor modeling. *Chemical Engineering Journal,* Volume 154(1-3)**,** pp. 25–33

Tesser, R., Casale, L., Verde, D., Di Serio, M., Santacesaria, E., 2010. Kinetics and modeling of fatty acids esterification on acid exchange resins. *Chemical Engineering Journal,* Volume 157(2-3)**,** pp. 539–550

Verziu, M., Coman, S.M., Richards, R., Parvulescu, V. I., 2011. Transesterification of vegetable oils over CaO catalysts. *Catalysis Today,* Volume 167(1)**,** pp. 64–70

Zavrazhnov, S.A., Esipovich, A.L., Zlobin, S.Y., Belousov, A.S. Vorotyntsev, A.V., 2019. Mechanism analysis and kinetic modelling of Cu NPs catalysed glycerol conversion into lactic acid. *Catalysts,* Volume 9(3)**,** p. 231

Zhang, Y., Wong, W.-T., Yung, K.-F., 2014. Biodiesel production via esterification of oleic acid catalyzed by chlorosulfonic acid modified zirconia. *Applied Energy,* Volume 116**,** pp. 191–198